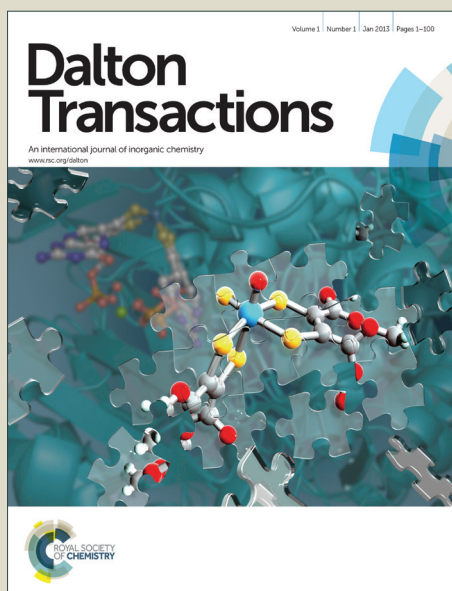


# Dalton Transactions

Accepted Manuscript



This is an *Accepted Manuscript*, which has been through the Royal Society of Chemistry peer review process and has been accepted for publication.

*Accepted Manuscripts* are published online shortly after acceptance, before technical editing, formatting and proof reading. Using this free service, authors can make their results available to the community, in citable form, before we publish the edited article. We will replace this *Accepted Manuscript* with the edited and formatted *Advance Article* as soon as it is available.

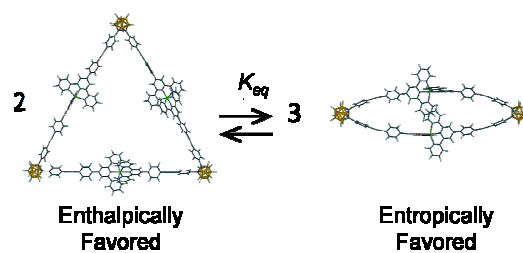
You can find more information about *Accepted Manuscripts* in the [Information for Authors](#).

Please note that technical editing may introduce minor changes to the text and/or graphics, which may alter content. The journal's standard [Terms & Conditions](#) and the [Ethical guidelines](#) still apply. In no event shall the Royal Society of Chemistry be held responsible for any errors or omissions in this *Accepted Manuscript* or any consequences arising from the use of any information it contains.

**Self-assembly of a family of suprametallomacrocycles:  
revisiting an *o*-carborane *bis*terpyridyl building block**

James M. Ludlow III, Masato Tominaga, Yoshiki Chujo, Anthony Schultz, Xiaocun Lu, Tingzheng Xie, Kai Guo, Charles N. Moorefield, Chrys Wesdemiotis,\* and George R. Newkome\*

Reaction of an *o*-carborane-based, *bis*terpyridyl building block with a labile metal gives mixtures of the enthalpically and entropically favored ring architectures and can be driven to the entropically favored product by dilution. NMR and ESI-TWIM-MS and molecular modeling afforded insights into the parameters affecting ring formation.



## ARTICLE

# Self-assembly of a family of suprametallomacrocycles: revisiting an *o*-carborane *bisterpyridyl* building block

Cite this: DOI: 10.1039/x0xx00000x

Received 00th January 2012,  
Accepted 00th January 2012

DOI: 10.1039/x0xx00000x

www.rsc.org/

James M. Ludlow III,<sup>a</sup> Masato Tominaga,<sup>d</sup> Yoshiki Chujo,<sup>d</sup> Anthony Schultz,<sup>b</sup> Xiaocun Lu,<sup>a</sup> Tingzheng Xie,<sup>a</sup> Kai Guo,<sup>a</sup> Charles N. Moorefield,<sup>c</sup> Chrys Wesdemiotis,<sup>\*a,b</sup> and George R. Newkome<sup>\*a,b</sup>

The self-assembly of the *o*-carborane-based, *bisterpyridyl* monomer, 1,2-*bis*[4'-(4-ethynylphenyl)-2,2':6',2''-terpyridine]-*o*-carborane, utilizing either Zn<sup>II</sup> or Fe<sup>II</sup> in a precise metal:ligand ratio (1:1), generated a family of metallomacrocycles that were studied *via* ESI-TWIM-MS, <sup>1</sup>H NMR, and 2D NMR (COSY, NOESY). Under kinetic control, *via* formation of Fe<sup>II</sup> complexes, the main cyclic product was triangular, as is typical of 60°-based *bis*ligands. Under thermodynamic control using more labile transition metal complexes, *e.g.* Zn<sup>II</sup>, the ratio of cyclic species was found to be concentration and temperature dependent, and under an adequate entropic driving force, the cyclic dimer was formed. This system was probed *via* variable temperature NMR to reveal dynamic equilibrium between the entropically favored dimer and enthalpically favored trimer.

## Introduction

Carborane-containing macromolecules exhibit several properties of interest, including chemical and thermal stability,<sup>1</sup> aggregation induced emission<sup>2</sup> (AIE), radiation shielding coatings<sup>3</sup> that enable their use in medical applications, and boron neutron capture therapy<sup>4,5</sup> (BNCT). Consequently, carboranes have been incorporated into a variety of macromolecular structures, including polymers<sup>2</sup> and dendrimers<sup>6-11</sup> in order to instill water-solubility and enhance their properties and utility. These approaches primarily rely upon covalent bonding; however, biomolecular systems exploit a range of weaker, non-covalent inter- and intra-molecular forces, including van der Waals, hydrogen bonding,  $\pi$ - $\pi$  stacking, electrostatic, and coordination to achieve macromolecular structure.<sup>12,13</sup> Notably, the incorporation of carborane into (metallo)supramolecular structures has received limited attention.<sup>13-16</sup>

Metal-ligand self-assembly has been utilized to form various metallosupramolecular structures including coordination polymers,<sup>1</sup> macrocycles,<sup>12-18</sup> and 3D structures.<sup>12,19</sup> The incorporation of [2,2':6',2'']terpyridine (tpy) has received increasing attention due in part to its ability to coordinate with

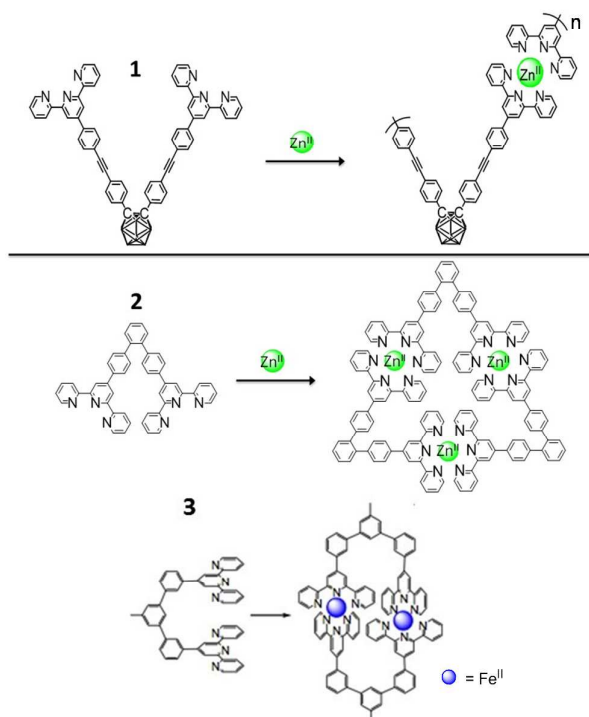


**Figure 1.** *Bisterpyridyl o*-carborane **1** and its reported<sup>2</sup> assembly with Zn<sup>II</sup>, reaction of a similar 60°-directed ligand **2** to give a triangle,<sup>18</sup> and assembly of parallel *bisterpyridine* **3** to generate a dimeric species.<sup>29</sup> [Redrawn with permission from the Royal Society of Chemistry: *Dalton Trans.* 2011, **40**, 1919-1923; *Dalton Trans.* 2012, **41**, 11573-11575; *Dalton Trans.* 2007, 626-628.]

<sup>a</sup>Department of Polymer Science, <sup>b</sup>Department of Chemistry, and <sup>c</sup>The Maurice Morton Institute for Polymer Science, The University of Akron, Akron, OH 44325-4717 USA. Tel: 330-972-6458

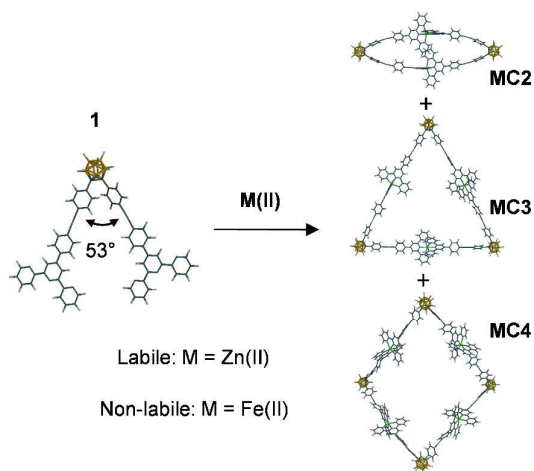
<sup>d</sup>Department of Polymer Chemistry, Graduate School of Engineering, Kyoto University, Katsura, Nishikyo-ku, Kyoto, 615-8510, Japan. Tel: +81-75-383-2604

†Electronic Supplementary Information (ESI) available: [includes 2D NMR spectra; ESI-MS and ESI-TWIM-MS; Isotope Patterns; van't Hoff plot and table]. See DOI: 10.1039/b000000x/

diverse transition metals permitting control of bond strengths, properties, and desired molecular architectures.<sup>20,21</sup> Terpyridine-based materials have found various applications, including supramolecular chemistry,<sup>12,22-24</sup> catalysis,<sup>25</sup> nanoparticles,<sup>26</sup> electroactive nanostructures,<sup>27</sup> and life science applications.<sup>20</sup> With metals that can form strong coordinative bonds, such as Os<sup>II</sup>, Ru<sup>II</sup>, and Fe<sup>II</sup>, the final product is kinetically determined by creation of irreversible <tpy-M<sup>II</sup>-tpy> complexes; in contrast, metals capable of more labile coordinative bonds, e.g. Zn<sup>II</sup> and Cd<sup>II</sup>, allow equilibration to the thermodynamic product.

Specific architectures are thus determined, in part, by building block geometry, e.g., the angle between conjoined ligands. Exploitation of the angular orientation and stoichiometric control of precursors is generally known as the directional bonding approach to supramolecular synthesis.<sup>12</sup> *Ortho*-carboranes possess an angle of ca. 53° between substituents attached to the two adjacent carbon atoms<sup>28</sup> and are thus well-suited for macrocyclizations, as has been reported with 60°-oriented *bis*ligands.<sup>18</sup>

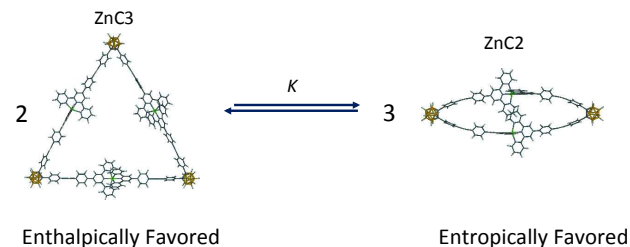
Chujo and Kokado recently reported<sup>2</sup> the synthesis and characterization of *bis*terpyridyl *o*-carborane **1**, which was subsequently complexed with Zn<sup>II</sup> (Figure 1) to give a coordination polymer that was investigated *via* <sup>1</sup>H NMR, UV-Vis, and fluorescence spectroscopies. The polymerization was also evaluated under various (metal-to-ligand) ratios. However, additional product characterization was not pursued with respect to possible discrete structure formation as is standard practice for polymeric reactions. With reports<sup>18</sup> detailing related 60°-based *bis*terpyridine ligands (e.g. **2**) that give almost exclusively cyclic structures, we investigated further.



**Scheme 1.** Complexation of ligand **1**: Conditions for **ZnC2-4**: Zn(OAc)<sub>2</sub>·2H<sub>2</sub>O, CHCl<sub>3</sub>:MeOH (4:1 v/v); and for **FeC2-4**: FeCl<sub>2</sub>, CHCl<sub>3</sub>:MeOH (3:2 v/v). Representations of the cyclic dimer (MC2), trimer (MC3), and tetramer (MC4).

In collaboration with the Chujo group, it was subsequently confirmed that, with a 1:1 metal to ligand ratio, *o*-carborane **1** forms predominately (85 %) macrocyclic structures, including the dimer, trimer, and tetramer along with minor polymeric and oligomeric species. To assess the self-assembly of **1** in a non-labile system, Fe<sup>II</sup> was used to form stable <tpy-Fe<sup>II</sup>-tpy>-based macrocycles (Scheme 1), which were easily separated by column chromatography. The ratio of trimer to dimer was ca. 8:1 with isolated yields of 30 and 4%. This indicates that the kinetic, cyclic product is a triangle, as is typical of a nominal 60° ligand, such as **1**. To assess self-assembly of **1** in a labile system, Zn<sup>II</sup> was used to form <tpy-Zn<sup>II</sup>-tpy> complexes. Variable temperature <sup>1</sup>H NMR and dilution studies indicated that the relative ratio of cyclic species was concentration and temperature dependent; whereas, with more dilute conditions and higher temperatures the dimer is favored. As well, sufficient dilution drove the system exclusively to the cyclic

dimer, a structure more characteristic of a *bis*-parallel ligand **3**. Furthermore, van't Hoff analysis indicated an equilibrium between the entropically favored dimer and the enthalpically favored trimer (Scheme 2). The resultant product distributions were characterized *via* ESI-TWIM-MS, <sup>1</sup>H NMR, and 2D NMR (COSY, NOESY). Molecular modeling was undertaken on the dimer, trimer, and tetramer species in order to obtain additional structural insights.



**Scheme 2:** Equilibrium between **ZnC3** (trimer) and **ZnC2** (dimer).

## Experimental

### Materials, synthesis, and analytical data

Chemicals were commercially purchased and used without further purification. Thin layer chromatography (TLC) was conducted on flexible sheets (Baker-flex) precoated with Al<sub>2</sub>O<sub>3</sub> (IB-F) or SiO<sub>2</sub> (IB2-F) and visualized by UV light. Column chromatography was conducted using basic Al<sub>2</sub>O<sub>3</sub>, Brockman Activity I (60-325 mesh) or SiO<sub>2</sub> (60-200 mesh) from Fisher Scientific. <sup>1</sup>H NMR spectra were recorded on a Varian 500 MHz spectrometer. Variable temperature NMR was conducted on a Varian 400 MHz NMR spectrometer; the temperature was varied from -40 to +70 °C in 10 °C increments. The temperature range was limited by the melting and boiling points of CD<sub>3</sub>CN. Electrospray ionization (ESI) mass spectra (MS) were obtained on a Synapt HDMS quadrupole/time-of-flight (Q/ToF) mass spectrometer (Waters Corp., Milford, MA). The Synapt Q/ToF instrument contains a travelling wave ion mobility (TWIM) device, in which ions drift under influence of a traveling wave field against the flow of the carrier gas (N<sub>2</sub>). This process disperses ions based on their mass, charge, and shape. The separated ions travel through a transfer cell from which they are conveyed to an orthogonal ToF analyzer for *m/z* measurement. The acquired data are typically displayed in 2-D plots of *m/z* ratio vs. the corresponding drift time through the IM cell. TWIM MS experiments were performed under the following conditions: ESI capillary voltage, 1 kV; sample cone voltage, 8 V; extraction cone voltage, 3.2 V; desolvation gas flow, 800 L/h (N<sub>2</sub>); trap collision energy (CE), 3 eV; transfer CE, 1 eV; trap gas flow, 1.5 mL/min (Ar); TWIM cell gas flow, 22.7 mL/min (N<sub>2</sub>); sample flow rate, 5 μL/min; source temperature, 30 °C; desolvation temperature, 40 °C; TWIM wave height, 7.5 V; and TWIM wave velocity, 350 m/s. TWIM data analyses were conducted using the MassLynx 4.1 and DriftScope 2.1 programs provided by Waters. Modeling and energy minimization of complexes were done with Spartan (Wavefunction, Inc.).

**Bis**terpyridyl *o*-carborane **1** was synthesized and characterized according to the literature<sup>2</sup> (Figure S1).

### Complex synthesis

**Zn<sub>n</sub>(1)<sub>n</sub>** (*n* = 2 - 4) (**ZnC2** - **ZnC4**): To a stirred solution of ligand **1** (23 mg, 24 μmol) in CHCl<sub>3</sub> (10 mL), was added a MeOH (2.4 mL) solution of Zn(OAc)<sub>2</sub>·2H<sub>2</sub>O (2.4 mL, 24 μmol), then stirred at 25 °C for 1 h. Excess NH<sub>4</sub>PF<sub>6</sub> was

## ARTICLE

added and stirred. The resultant cream-colored precipitate was filtered and washed with copious amounts of MeOH to give (85 %) complex **Zn<sub>n</sub>(1)<sub>n</sub>**: 24 mg, m.p. >300 °C; <sup>1</sup>H NMR (CD<sub>3</sub>CN, 500 MHz): δ = 8.99 (s), 8.93 (s), 8.73 (d, *J* = 8 Hz), 8.62 (d, *J* = 8 Hz), 8.24 (d, *J* = 9 Hz), 8.15 – 8.22 (m), 7.81 – 7.97 (m), 7.73 (d, *J* = 5 Hz), 7.68 (d, *J* = 9 Hz), 7.64 (d, *J* = 9 Hz), 7.52 (d, *J* = 9 Hz), 7.47 (d, *J* = 9 Hz), 7.41 (dd, *J*<sub>1</sub> = 9 Hz, *J*<sub>2</sub> = 5 Hz), 7.19 (dd, *J*<sub>1</sub> = 9 Hz, *J*<sub>2</sub> = 5 Hz), 2.30 – 3.00 ppm (br m, B-H); ESI-MS (*m/z*) **ZnC2**: 512.2 [M-4PF<sub>6</sub>]<sup>4+</sup> (Calcd. *m/z* = 512.2), 731.2 [M-3PF<sub>6</sub>]<sup>3+</sup> (Calcd. *m/z* = 731.3), 1169.3 [M-2PF<sub>6</sub>]<sup>2+</sup> (Calcd. *m/z* = 1169.4); **ZnC3**: 643.4 [M-5PF<sub>6</sub>]<sup>5+</sup> (Calcd. *m/z* = 643.4), 841.0 [M-4PF<sub>6</sub>]<sup>4+</sup> (Calcd. *m/z* = 841.0); **ZnC4**: 1607.5 [M-3PF<sub>6</sub>]<sup>3+</sup> (Calcd. *m/z* = 1607.4)

**Fe<sub>n</sub>(1)<sub>n</sub>** (*n* = 2-4): To a stirred CHCl<sub>3</sub>:MeOH (3:2 v/v, 300 mL) solution, **1** (28 mg, 29.2 μmol) was added, then a MeOH solution of FeCl<sub>2</sub>·4H<sub>2</sub>O (2.92 mL, 29.2 μmol) was added dropwise. After stirring at 25 °C for 16 h, the reaction mixture was concentrated *in vacuo* to give a purple solid, which was column chromatographed (SiO<sub>2</sub>) using H<sub>2</sub>O/MeCN/satd. KNO<sub>3(aq)</sub> (1:30:1; v/v/v) to give the cyclic dimer (R<sub>f</sub> = 0.15) and trimer (R<sub>f</sub> = 0.07). Counterion exchange to PF<sub>6</sub><sup>-</sup> was achieved by dissolving the complex in CHCl<sub>3</sub>:MeOH (1:1 v/v) and precipitating with NH<sub>4</sub>PF<sub>6</sub>. ESI-MS and <sup>1</sup>H NMR were performed with a PF<sub>6</sub><sup>-</sup> counterion.

**Dimer [Fe<sub>2</sub>(1)<sub>2</sub>] (FeC2)**: 1.5 mg (4%); <sup>1</sup>H NMR (CD<sub>3</sub>CN, 500 MHz): δ = 9.08 (s, 3',5'-tpyH, 8H), 8.41 (d, *J* = 8 Hz, 3,3''-tpyH, 8H), 8.29 (d, *J* = 8 Hz, ArH, 8H), 7.92 (d, *J* = 8 Hz, ArH, 8H), 7.63 (d, *J* = 8 Hz, ArH, 8H), 7.45 (d, *J* = 8 Hz, ArH, 8H), 7.27 (dd, *J*<sub>1</sub> = *J*<sub>2</sub> = 8 Hz, 4,4''-tpyH, 8H), 7.00 (d, *J* = 6 Hz, 6,6''-tpyH, 8H), 6.70 (dd, *J*<sub>1</sub> = 8 Hz, *J*<sub>2</sub> = 6 Hz, 5,5''-tpyH, 8H), 2.32 – 2.95 ppm (br m, B-H); ESI-MS (*m/z*): 725.2 [M-3PF<sub>6</sub>]<sup>3+</sup> (Calcd *m/z* = 725.2), 507.7 [M-4PF<sub>6</sub>]<sup>4+</sup> (Calcd *m/z* = 507.7)

(CD<sub>3</sub>CN, 500 MHz): δ = 9.17 (s, 3',5'-tpyH, 12 H), 8.60 (d, *J* = 8 Hz, 3,3''-tpyH, 12H), 8.35 (d, *J* = 8 Hz, ArH, 12H), 7.95 (d, *J* = 9 Hz, ArH, 12H), 7.89 (dd, *J*<sub>1</sub> = *J*<sub>2</sub> = 8 Hz, 4,4''-tpyH, 12H), 7.66 (d, *J* = 8 Hz, ArH, 12H), 7.51 (d, *J* = 8 Hz, ArH, 12H), 7.17 (d, *J* = 6 Hz, 6,6''-tpyH, 12H), 7.06 (dd, *J*<sub>1</sub> = 8 Hz, *J*<sub>2</sub> = 6 Hz, 5,5''-tpyH, 12H), 2.24 – 3.00 ppm (br m, B-H); <sup>13</sup>C NMR (125 MHz, CD<sub>3</sub>CN): δ = 85.47, 89.98, 91.31, 121.69, 124.09, 124.9, 125.37, 127.55, 128.38, 130.70, 131.5, 131.76, 133.00, 137.24, 138.97, 149.51, 153.25, 158.13, 160.59 ppm; ESI-MS (*m/z*): 507.6 [M-6PF<sub>6</sub>]<sup>6+</sup> (Calcd *m/z* = 507.5), 638.0 [M-5PF<sub>6</sub>]<sup>5+</sup> (Calcd *m/z* = 638.0), 833.9 [M-4PF<sub>6</sub>]<sup>4+</sup> (Calcd *m/z* = 833.8), 1160.1 [M-3PF<sub>6</sub>]<sup>3+</sup> (Calcd *m/z* = 1160.0)

**Tetramer [Fe<sub>4</sub>(1)<sub>4</sub>] (FeC4)**: Not isolated but detected *via* ESI-MS (*m/z*): 600.7 [M-7PF<sub>6</sub>]<sup>7+</sup> (Calcd *m/z* = 600.7).

## Results and Discussion

### <sup>1</sup>H NMR of Zinc Complexes

Following reaction of the bisligand **1** with Zn(OAc)<sub>2</sub> to give **Zn<sub>n</sub>(1)<sub>n</sub>**, the <sup>1</sup>H NMR spectrum revealed two sets of terpyridine resonances with an integration ratio of *ca.* 0.8:1 suggesting that there are multiple species present. The <sup>1</sup>H NMR spectrum was consistent with the presence of cyclic structures where the 6,6'' tpyH signals shifted upfield from 8.75 ppm to 7.73 and 7.85 ppm (Figure 2), which is indicative of a bisterpyridine Zn<sup>II</sup> complex. COSY <sup>1</sup>H NMR confirmed two discrete sets of terpyridine protons (Figure S2).

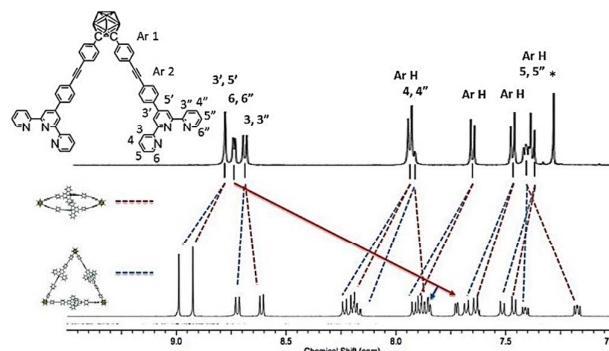


**Figure 2.** 500MHz <sup>1</sup>H NMR spectra. Top – ligand **1** (CDCl<sub>3</sub>) and bottom – **Zn<sub>n</sub>(1)<sub>n</sub>** in CD<sub>3</sub>CN. (\*- CHCl<sub>3</sub>)

### Mass Spectrometry of the Zinc Complexes

Multiple species were observed *via* ESI-MS including dimer (**ZnC2**), trimer (**ZnC3**), and tetramer (**ZnC4**) (Figure 3). The most prominent peaks correspond to the 4+, 3+, and 2+ states of the cyclic dimer, which was initially unexpected.

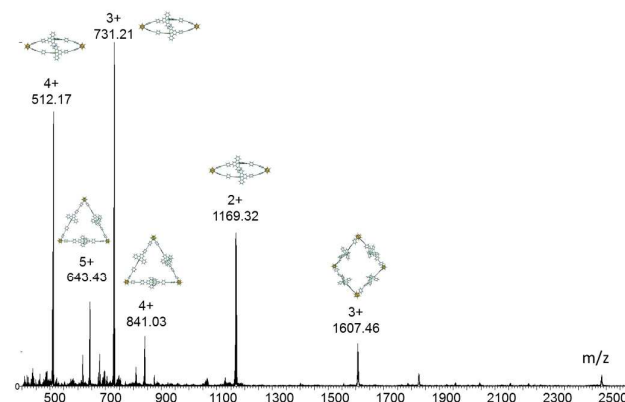


**Figure 3.** ESI – MS of zinc complexes (**ZnC2**-**ZnC4**) at 0.6 mg/mL.

### Effects of Concentration on the Zinc Complexes

The **Zn<sub>n</sub>(1)<sub>n</sub>** system showed concentration dependence; thus, a dilution study was performed in CD<sub>3</sub>CN. <sup>1</sup>H NMR spectra were taken at each concentration and the relative proportion of cyclic species was assessed *via* integration of the two 3',5' singlets (Figure 4). Upon dilution, the singlet at 8.99 ppm diminishes relative to the singlet at 8.93 ppm indicating an equilibrium shift toward the dimer relative to the trimer. And, the <sup>1</sup>H NMR and ESI-MS data showed the dimer **ZnC2** as the major product (Figures 4 and 5).

ESI-MS analysis of a dilute solution of **Zn<sub>n</sub>(1)<sub>n</sub>** (20 μg/mL) supports the presence of the dimer **ZnC2** (Figure 5). Thus, the more shielded set of protons is exclusively from the dimer. This shift to an entropically favored species follows Le Chatelier's Principle. As concentration is decreased, the system responds by shifting the equilibrium toward the species assembled with fewer components. The sharp, distinct peaks from each set of tpy protons indicate a rapid equilibrium between molecular architectures relative to the NMR time scale.

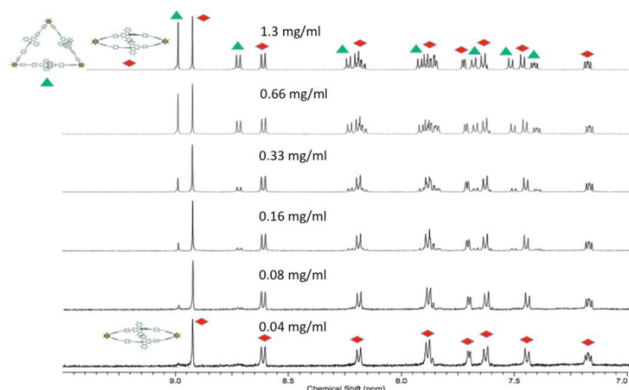


**Figure 4.** Dilution effect on ratio of **ZnC2** to **ZnC3**. Each subsequent spectrum was measured after 1:1 dilution with  $\text{CD}_3\text{CN}$ .

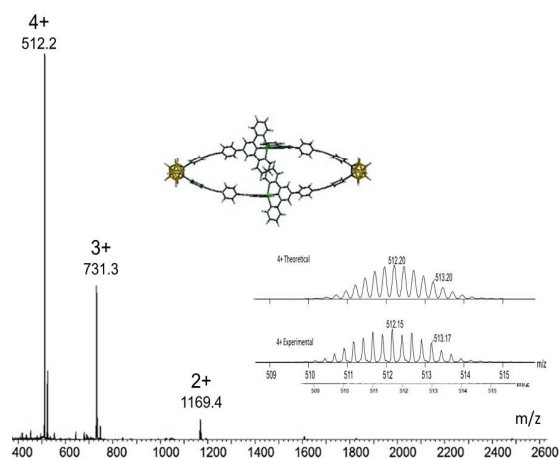


**Figure 5.** ESI-MS of **ZnC2** under dilute conditions ( $[\text{Zn}_n(\text{I})_n] = 20 \mu\text{g/mL}$ ) showing only the dimeric species, along with the theoretical and experimental isotope patterns of the 4+ charge state.

### Effect of Temperature on the Zinc Complexes

As the temperature was lowered, the chemical shift of the trimer signals remains unchanged; however, the 4,4'' and 5,5'' peaks of **ZnC2** shifted upfield (Figure 6). This chemical shift was also observed in a previous report about interlocked <tpy- $\text{M}^{\text{II}}$ -tpy> complexes.<sup>29</sup> This result implies that, as molecular motion is decreased, the shielding effect from the cyclic dimer's unique structure is enhanced. Conversely, the environment of the aromatic protons of **ZnC3** is much less sensitive to the degree of molecular motion. Previous reports indicate that the proton signals of cyclic <tpy- $\text{M}^{\text{II}}$ -tpy> trimers assembled from 60° ligands show negligible change in chemical shift when the temperature is varied.<sup>30</sup>

Temperature also affected the relative proportions of cyclic species as measured *via* integration of the respective 3',5' peaks; increasing temperature produced higher proportions of the dimeric species (**ZnC2**). At 70 °C, the ratio of the 3',5' peak of **ZnC2** to the 3',5' peak of **ZnC3** was 1:0.8; whereas, at -40 °C, the ratio was 1:1.3. The entropic driving force is proportional to temperature; thus, higher temperatures favor the dimeric construct. The shift toward dimer at higher temperatures also suggests that its formation is endothermic. At lower temperatures, peak broadening is indicative of the slowing equilibrium between molecular architectures relative to the NMR timescale.

The variable temperature NMR data were used to estimate the enthalpic and entropic components of the equilibrium. Mole

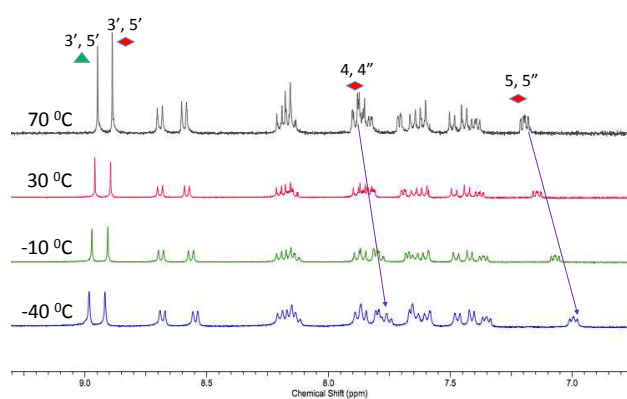


**Figure 6.** Variable temperature  $^1\text{H}$  NMR of **Zn<sub>n</sub>(I)<sub>n</sub>** study on a 400 MHz spectrometer in  $\text{CD}_3\text{CN}$ .

fractions were derived from integration of each 3',5' peaks. The assumption was made that the upfield peak represents trimer, exclusively. This assumption is safest at the higher end of the temperature range studied so the data from 10 – 70 °C was used. Assuming ideal behavior,  $K_{\text{eq}}$  for the equilibrium shown in Scheme 2 can be written:

$$K_{\text{eq}} = \frac{\{\text{dimer}\}^3}{\{\text{triangle}\}^2} \quad (1)$$

The van't Hoff equation is shown in (2).

$$\ln K_{\text{eq}} = -\frac{\Delta H_{\text{eq}}}{RT} + \frac{\Delta S_{\text{eq}}}{R} \quad (2)$$

A van't Hoff plot was constructed and analyzed (Figure S10).  $\Delta H_{\text{eq}}$  for conversion of two triangles into three dimers was found to be positive (*ca.* 12 kJ/mol) indicating that dimer formation is endothermic and suggesting that the cyclic dimer is the more strained structure.  $\Delta S_{\text{eq}}$  was positive (*ca.* 40 J/mol K) reflecting the increase in the number of macrocycles, as the equilibrium shifts to the dimeric species. These results are similar to dynamic equilibration reported between triangles and squares in labile systems such as  $\text{Pd}^{\text{II}}$  and  $\text{Pt}^{\text{II}}$  with linear (180°) *bis*pyridyl ligands.<sup>31-36</sup> Equilibrium pairs between dimeric and trimeric species are uncommon but have been reported.<sup>37</sup> This is, to the best of our knowledge, the first reported cyclic dimer-trimer equilibrium driven *via* <tpy- $\text{M}^{\text{II}}$ -tpy> complexation.

### Iron Complexes

In order to isolate and study non-labile analogues of these cyclic species, **1** was reacted with  $\text{FeCl}_2$  to generate <tpy- $\text{Fe}^{\text{II}}$ -tpy> complexes, which are stable and separable *via* chromatography. ESI-MS of the crude reaction mixture revealed formation of a variety of cyclic species - primarily dimer, trimer, and tetramer (Figure 7). The most prominent species in the spectra is trimer, **FeC3**, showing charge states 3+ through 6+. Larger macrocycles, such as pentamer and hexamer, were detected at trace levels.

The dimer and trimer species were isolated chromatographically on  $\text{SiO}_2$  using  $\text{H}_2\text{O}/\text{MeCN}/\text{sat'd KNO}_3(\text{aq})$  (1:30:1; v/v/v) and then converted to  $\text{PF}_6^-$  salts. The trimer was the main cyclic product isolated as would be expected of a nominal 60° ligand. Both products were characterized by  $^1\text{H}$  NMR (Figure 8) and ESI-TWIM-MS (Figures 9 and S7).

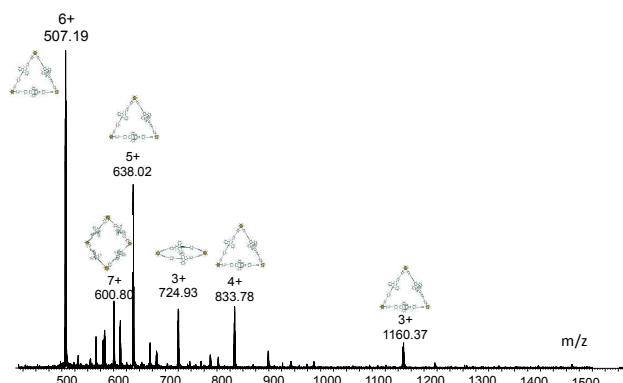


**Figure 7.** ESI-MS of the Fe(II) reaction mixture after precipitation with  $\text{NH}_4\text{PF}_6$ . Peaks for  $\text{FeC2}$  –  $\text{FeC4}$  are marked.

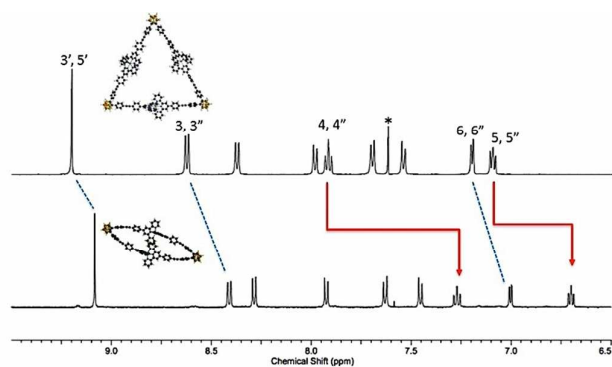


**Figure 8.**  $^1\text{H}$  NMR spectra of the cyclic dimer  $\text{FeC2}$  (bottom) and trimer  $\text{FeC3}$  (top) in  $\text{CD}_3\text{CN}$ . (\* $\text{CHCl}_3$ )

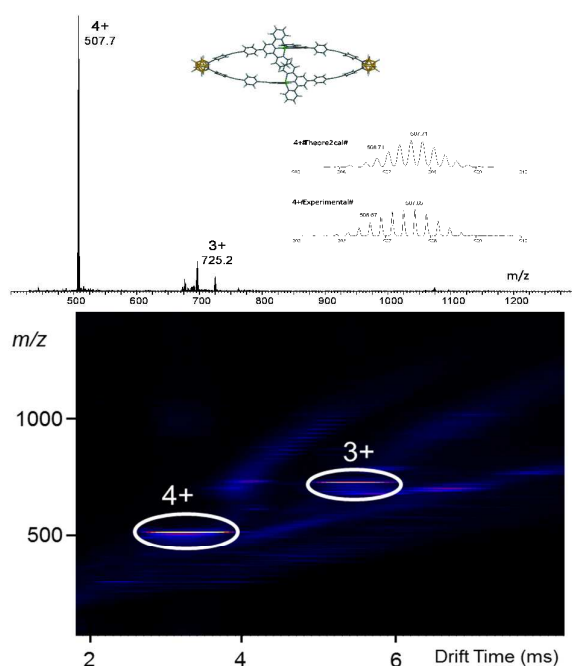


**Figure 9.** ESI-MS spectrum for  $\text{FeC2}$  (1) (top) and 2D ESI-TWIM-MS plot (m/z vs. drift time) for  $\text{FeC2}$  (bottom).

$^1\text{H}$  NMR spectra of both species are consistent with a cyclic structure, as the 6,6'' signals are shifted upfield, indicative of *bisterpyridine* complex formation. The terpyridine protons of the complexed dimer show a dramatic upfield shift relative to those of the trimer, particularly the 4,4'' and 5,5'' protons. This

observed difference can be attributed to the more highly shielded proton environment that results from proximity interactions of the dimer's complexes as seen in molecular models. The sharp tpy proton resonances observed in the dimer spectra also suggest correlated rotation of the close complexes at a rate greater than the NMR timescale. Note that superposition of these spectra would match the pattern seen with the initial zinc system, *i.e.*, two distinct sets of tpy protons and that the dimeric species is further upfield. Assignments were confirmed *via* COSY and NOESY (Figures S3-5 in Supplemental Information).

Figure 9 (top) shows the ESI-MS spectrum for the  $\text{FeC2}$  species, which includes the 4+ and 3+ charge states as well as theoretical and experimental isotope patterns for the 4+ charge state. The ESI-TWIM-MS plot (bottom) shows the expected step pattern and does not indicate the presence of superimposed isomers or conformers. Similar results were observed for the  $\text{FeC3}$  species (Figure S7).

Experimental Collisional Cross Sections (CCSs)<sup>17, 38-42</sup> were calculated based on TWIM data to further characterize the different architectures (Table 1). Relative CCSs for these architectures show a linear trend with respect to mass. Energy minimized structures were generated for  $\text{FeC2}$ ,  $\text{FeC3}$ , and  $\text{FeC4}$  *via* simulated annealing. Theoretical CCS values were calculated *via* the projection approximation (PA) method using MOBCAL and found to be  $443 \pm 3$ ,  $720 \pm 2$ , and  $925 \pm 11 \text{ \AA}^2$  for  $\text{FeC2}$ ,  $\text{FeC3}$ , and  $\text{FeC4}$ , respectively, corresponding well with experimental values. The population of model structures for both  $\text{FeC3}$  and  $\text{FeC4}$  each included a set of folded conformations showing intramolecular  $\pi$ - $\pi$  interactions. Their CCS values were calculated separately and found to be  $580 \pm 40$  and  $668 \pm 40 \text{ \AA}^2$ , respectively.

Z	CCS ( $\text{\AA}^2$ )		
	FeC2	FeC3	FeC4
3+	507	723	-
4+	496	770	-
5+	-	805	-
6+	-	756	-
7+	-	-	1068
Average	502	764	1068
Std. Dev.	8	34	-

**Table 1:** Experimental Collision Cross Sections (CCSs) of  $\text{FeC2}$ ,  $\text{FeC3}$ , and  $\text{FeC4}$ .

## Molecular Modeling

Molecular modeling provided insight into experimental findings, including the proton shifts relative to the trimer and ligand's ability to behave similarly to a *bis* parallel ligand. Figure 10 shows the cyclic dimer, the planar cyclic trimer, and the folded cyclic tetramer.

The tetramer architecture is analogous to previously reported Dondorff rings.<sup>43</sup> The folded conformation of the tetramer reduces strain relative to a planar conformation and is typical for a nominal  $60^\circ$  bis-ligand. The angle between the ligand arms is essentially the same as for the trimer; thus, there is little or no enthalpic penalty to its formation. Cyclic dimer species are generally formed from *bis* parallel ligands such as **3**. A cyclic dimer such as this has not been previously reported with  $60^\circ$  oriented *bisterpyridyl* ligands. Side-on and end-on views of the dimer are depicted in Figure 11.

The model indicates that the ligand arms must adopt a tighter, more strained angle (*ca.*  $30^\circ$ ) to form the cyclic dimer. The inner 4,4'' and 5,5'' protons are projected into the adjacent complex unit and should be more highly shielded than in the cyclic trimer. In Figure 2, the  $^1\text{H}$  NMR of this cyclic dimer showed significant upfield shifting of

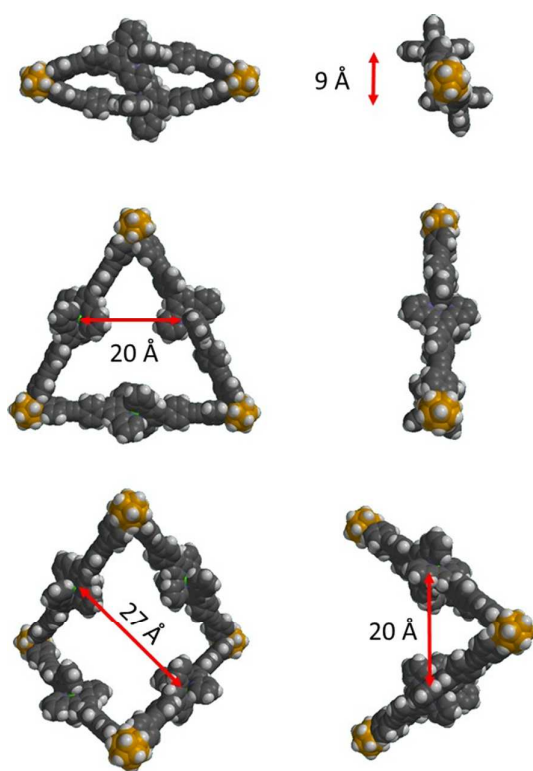


**Figure 10.** Space-filling models of **FeC2**, **FeC3**, and **FeC4**: top view (left) and side view (right). Color scheme: B: yellow; H: white; C: grey; N: purple; Fe: green; Fe-Fe distances are shown with red arrows.

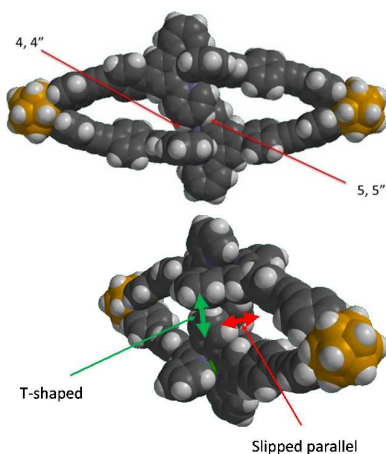


**Figure 11.** Space filling models of **FeC2** showing interlocked  $\langle \text{tpy-M}^{\text{II}}\text{-tpy} \rangle$  complexes. Color scheme: B: yellow; H: white; C: grey; N: purple; Fe: green. 4, 4'' and 5, 5'' protons are noted (top). Regions of T-shaped (CH- $\pi$ ) and slipped parallel ( $\pi$ - $\pi$ ) interactions are noted (bottom).

the complexed 4,4'' and 5,5'' protons relative to the trimer as expected for a close-packed, metal-terpyridine moiety.  $^1\text{H}$  NMR also gave a very crisp, single set of tpy protons and yet the model shows that the 4,4'' and 5,5'' protons are also exposed to a non-shielded exterior of the molecule. This suggests gear-like correlated rotation of the intertwined complexes. These results match with observations seen in previous interlocked species.<sup>29,44</sup> Both slipped parallel ( $\pi$ - $\pi$ ) and T-shaped (CH- $\pi$ ) stacking interactions can be envisioned. Dimensions of the model also match closely those reported<sup>29</sup> for interacting tpy complexes formed from *bis*parallel ligands. For example, the metal to metal distance in **FeC2** is *ca.* 9 Å vs. 8.8 Å in the

reported complex and  $\pi$ - $\pi$  stacking distance in **FeC2** is *ca.* 4 Å vs. reported 3.7-3.9 Å for the reported complex.

Factors contributing to the ability of this ligand to form a cyclic dimer include: 1) inherent flexibility of the alkyne moieties, 2) favorable  $\pi$ - $\pi$  and CH- $\pi$  interactions between the interacting complexes, 3) length of the arm possessing two phenyls and an alkyne spacer, and 4) 53° angle and C-C bond length of *o*-carborane.

Though the alkyne group is generally linear, it is flexible as exhibited in cyclooctyne and larger cycloalkynes, where the alkyne group can adopt a *cisoid* bend due to covalent bonding constraints. In the case of cyclodecyne, the internal strain is reported to be *ca.* 20 kJ/mol.<sup>45</sup> So, while there would be an energetic penalty to adopting the more strained conformation of the dimer - it is not prohibited. Conversely, the  $\pi$ - $\pi$  interactions upon dimer formation should be energetically favorable at a similar magnitude. Such  $\pi$ - $\pi$  interactions are generally described as parallel, T-shaped, and slipped-parallel and their respective energies reported<sup>46</sup> to be -6.2, -10.3, and -10.4 kJ/mol respectively. In the specific case of  $\pi$  stacking between *bis*terpyridine-metal complexes, evidence for its favorability is seen in Constable's examples, where the complexes interact, even when the spacers linking *bis*terpyridines are long and highly flexible.<sup>44</sup> Therefore, the enthalpic penalty of forming these more strained dimers is likely offset to some degree by favorable  $\pi$ - $\pi$  and CH- $\pi$  interactions. Also, adequate arm length *via* two phenyl spacers removes steric obstruction to dimer formation and, though the alkyne is the most flexible part of the arm, it does provide additional structure for strain distribution. Molecular modeling also indicates slight bending of the phenyl rings in the dimer. Characteristics unique to carborane also likely play a role. Relative to the phenyl ring in a ligand such as **1**, *o*-carborane has more narrow bite angle (53° vs. 60°) and longer C to C bond length. While the phenyl C to C bond length is *ca.* 1.4 Å, in carborane the C to C bond is reported<sup>47</sup> to range from 1.65 to 1.75 Å in the crystal state, indicating that it is not only longer but can adopt a variety of lengths depending upon conditions.

## Conclusions

The self-assembly characteristics of the recently reported<sup>2</sup> *bis*terpyridyl *o*-carborane **1** were examined and it was found to undergo macrocyclizations when reacted with  $\text{Zn}^{\text{II}}$  and  $\text{Fe}^{\text{II}}$ ; characterization was achieved by NMR, ESI- and ESI-TWIM-MS, and molecular modeling. More specifically, using a 1:1 metal-to-ligand ratio, the cyclic dimer, trimer, and tetramer were confirmed as major products. Under kinetic control, *i.e.* for the  $\text{Fe}^{\text{II}}$  complexes, the predominant cyclic product was trimeric; whereas, under thermodynamic control, *i.e.* for the  $\text{Zn}^{\text{II}}$  complexes, ligand **1** formed the dimer exclusively, given adequate entropic driving force. Molecular modeling suggests that the ligand's alkyne moieties, arm length, and favorable  $\pi$ - $\pi$  interactions, upon complexation, play a role in enabling this unique behavior. Notably, the potential to obtain discrete products from polymeric-type reactions should be considered, as has been observed in other cases, where polydentate ligands were present.<sup>44,48-50</sup>

## Acknowledgments

Support is acknowledged from the National Science Foundation (CHE-1151991 to GRN and CHE-1012636 to CW) and The University of Akron. We thank Nicholas Johnson for his valuable assistance and expertise with the variable temperature NMR experiments.

## Notes and references

- W. Jiang, C. B. Knobler, M. D. Mortimer and M. F. Hawthorne, *Angew. Chem.*, 1995, **35**, 1332-1334.
- K. Kokado and Y. Chujo, *Dalton Trans.*, 2011, **40**, 1919-1923.
- A. Herzog, A. Maderna, G. N. Harakas, C. B. Knobler and M. F. Hawthorne, *Chem. Eur. J.*, 1999, **5**, 1212-1217.
- M. F. Hawthorne, *Angew. Chem. Int. Ed.*, 1993, **32**, 950-984.
- R. F. Barth, A. H. Soloway and R. G. Fairchild, *Cancer Res.*, 1990, **50**, 1061-1070.
- G. R. Newkome, C. N. Moorefield, J. M. Keith, G. R. Baker and G. H. Escamilla, *Angew. Chem. Int. Ed.*, 1994, **33**, 666-668.
- C. B. Gorman, B. L. Parkhurst, W. Y. Su and K.-Y. Chen, *J. Am. Chem. Soc.*, 1997, **119**, 1141-1142.
- R. Djeda, J. Ruiz, D. Astruc, R. Satapathy, B. P. Dash and N. S. Hosmane, *Inorg. Chem.*, 2010, **49**, 10702-10709.
- B. P. Dash, R. Satapathy, B. P. Bode, C. T. Reidl, J. W. Sawicki, A. J. Mason, J. A. Maguire and N. S. Hosmane, *Organometallics*, 2012, **31**, 2931-2935.
- A. G. Campo, C. Vinas, F. Teixodor, R. Nunez, R. Sillanpää and R. Kivekäs, *Macromolecules*, 2007, **40**, 5644-5652.
- N. S. Hosmane, Z. Yinghui, J. A. Maguire, W. Kaim and M. Takagaki, *J. Organomet. Chem.*, 2009, **694**, 1690-1697.
- R. Chakrabarty, P. S. Mukherjee and P. J. Stang, *Chem. Rev.*, 2011, **111**, 6810-6918.
- B. H. Northrop, H.-B. Yang and P. J. Stang, *Chem. Commun.*, 2008, **45**, 5896-5908.
- H. Jude, H. Disteldorf, S. Fischer, T. Wedge, A. M. Hawkrige, A. M. Arif, M. F. Hawthorne, D. C. Muddiman and P. J. Stang, *J. Am. Chem. Soc.* 2005, **127**, 12131-12139.
- N. Das, P. J. Stang, A. M. Arif and C. F. Campana, *J. Org. Chem.* 2005, **70**, 10440-10446.
- Z.-J. Yao, W.-B. Yu, Y.-J. Lin, S.-L. Huang, Z.-H. Li and G.-X. Jin, *J. Am. Chem. Soc.*, 2014, **136**, 2825-2832.
- J.-L. Wang, X. Li, X. Lu, I.-F. Hsieh, Y. Cao, C. N. Moorefield, C. Wesdemiotis, S. Z. D. Cheng and G. R. Newkome, *J. Am. Chem. Soc.* 2011, **133**, 11450-11453.
- A. Schultz, Y. Cao, M. Huang, S. Z. D. Cheng, X. Li, C. N. Moorefield, C. Wesdemiotis and G. R. Newkome, *Dalton Trans.*, 2012, **41**, 11573-11575.
- X. Lu, X. Li, Y. Cao, A. Schultz, J.-L. Wang, C. N. Moorefield, C. Wesdemiotis, S. Z. D. Cheng and G. R. Newkome, *Angew. Chem. Int. Ed.* 2013, **52**, 7728-7731.
- U. S. Schubert, A. Winter and G. R. Newkome, *Terpyridine-based Materials - For Catalytic, Optoelectronic, and Life Science Applications*, Wiley-VCH, Weinheim, Germany, 2011.
- U. S. Schubert, H. Hofmeier and G. R. Newkome, *Modern Terpyridine Chemistry*, Wiley-VCH, Weinheim, Germany, 2006.
- E. C. Constable, *Chem. Soc. Rev.*, 2007, **36**, 246-253.
- E. C. Constable, *Coord. Chem. Rev.*, 2008, **252**, 842-855.
- I. Eryazici, C. N. Moorefield and G. R. Newkome, *Chem. Rev.*, 2008, **108**, 1834-1895.
- A. Winter, G. R. Newkome and U. S. Schubert, *ChemCatChem*, 2011, **3**, 1384-1406.
- A. Winter, M. D. Hager, G. R. Newkome and U. S. Schubert, *Adv. Mater.*, 2011, **23**, 5728-5748.
- A. Winter, S. Hoepfner, G. R. Newkome and U. S. Schubert, *Adv. Mater.*, 2011, **23**, 3484-3498.
- M. A. Fox, J. A. K. Howard, J. A. H. MacBride, A. Mackinnon and K. Wade, *J. Organomet. Chem.*, 2003, **680**, 155-164.
- I. Eryazici, P. Wang, C. N. Moorefield, M. Panzer, S. Durmus, C. D. Shreiner and G. R. Newkome, *Dalton Trans.*, 2007, 626-628.
- A. Schultz, X. Li, C. N. Moorefield, C. Wesdemiotis and G. R. Newkome, *Eur. J. Inorg. Chem.*, 2013, 2492-2497.
- M. Schweiger, S. R. Seidel, A. M. Arif and P. J. Stang, *Inorg. Chem.*, 2002, **41**, 2556-2559.
- M. Ferrer, M. Mounir, O. Rossell, E. Ruiz and M. A. Maestro, *Inorg. Chem.* 2003, **42**, 5890-5899.
- A. Sautter, D. G. Schmid, G. Jung and F. Wu, *J. Am. Chem. Soc.*, 2001, **123**, 4524-4530.
- C. A. Schalley, T. Müller, P. Linnartz, M. Witt, M. Schäfer and A. Lützen, *Chem. Eur. J.*, 2002, **8**, 3538 - 3551.
- T. Weilandt, R. W. Troff, H. Saxell, K. Rissanen and C. A. Schalley, *Inorg. Chem.*, 2008, **47**, 7588-7598.
- M. Fujita, O. Sasaki, T. Mitsuhashi, T. Fujita, J. Yazaki, K. Yamaguchi and K. Ogura, *Chem. Commun.*, 1996, 1535-1536.
- M. Fujita, M. Aoyagi and K. Ogura, *Inorg. Chim. Acta* 1996, **246**, 53-57.
- J. Thiel, D. Yang, M. N. Rosnes, X. Liu, C. Yvon, S. E. Kelly, Y.-F. Song, D.-L. Long and L. Cronin, *Angew. Chem. Int. Ed.*, 2011, **50**, 8871-8875.
- M. T. Bowers, P. R. Kemper, G. von Helden and P. A. M. van Koppen, *Science* 1993, **260**, 1446-1451.
- E. R. Brouck, S. E. Anderson, B. H. Northrop, P. J. Stang and M. T. Bowers, *J. Am. Chem. Soc.*, 2010, **132**, 13486-13494.
- Y.-T. Chan, X. Li, J. Yu, G. A. Carri, C. N. Moorefield, G. R. Newkome and C. Wesdemiotis, *J. Am. Chem. Soc.*, 2011, **133**, 11967-11976.
- J. Ujima, M. D. Cecco, O. Chepelin, H. Levene, C. Moffat, S. J. Pike, P. J. Lusby and P. E. Barran, *Chem. Commun.*, 2012, **48**, 4423 - 4425.
- A. Schultz, X. Li, J. K. McCusker, C. N. Moorefield, F. N. Castellano, C. Wesdemiotis and G. R. Newkome, *Chem. Eur. J.*, 2012, **18**, 11569-11572.
- E. C. Constable, C. E. Housecroft, M. Neuburger, S. Schaffner and C. B. Smith, *Dalton Trans.*, 2005, 2259-2267.
- J. D. Roberts and M. C. Caserio, *Basic Principles of Organic Chemistry*, Benjamin, Inc., Menlo Park, CA, 1977.
- S. Tsuzuki, K. Honda, T. Uchimaru, M. Mikami and K. Tanabe, *J. Am. Chem. Soc.*, 2001, **124**, 104-112.
- L. Weber, J. Kahlert, L. Bohling, A. Brockhinke, H.-G. Stammel, B. Neumann, R. A. Harder, P. J. Low and M. A. Fox, *Dalton Trans.*, 2013, **42**, 2266-2281.
- D. G. Kurth, F. Caruso, C. Schüller, *Chem. Commun.*, 1999, 1579-1580.
- V. A. Friese, D. G. Kurth, *Curr. Opin. Colloid In.*, 2009, **14**, 81-93.
- S. Chen, J. Duhamel, *J. Phys. Chem. B*, 2011, **115**, 3289-3302.